Real-time Control of HCCI Engine Using Model Predictive Control

Khashayar Ebrahimi[1*] and C R Bob Koch[1]

[1]Department of Mechanical Engineering, University of Alberta, Edmonton, AB, T6G 1H9, Canada
Email: ebrahimi@ualberta.ca

Abstract— **Model Predictive Control (MPC) for combustion timing and load control of a single cylinder Homogeneous Charge Compression Ignition (HCCI) engine is designed and implemented. First, a nonlinear control oriented model is obtained based on a Detailed Physical Model (DPM) using model order reduction techniques. The model is then linearized around one operating point and combustion timing and output work prediction are experimentally validated. This linearized model is then used in MPC with Exhaust Valve Closing (EVC) timing and fueling rate as main actuators. Combustion timing is defined as the crank angle of fifty percent fuel mass fraction burned, and is calculated from cylinder pressure. The controller is verified in simulation using the DPM considering constraints on inputs and outputs. The controller is then directly implemented on a dSPACE MicroAutoBox for HCCI combustion timing and load control. For real-time implementation of the MPC, Laguerre functions are used to simplify the conventional MPC algorithm which reduces the computation time. The MPC tracks the desired load and combustion timing trajectories while considering constraints on the actuators and outputs in simulation and on the engine.**

I. Introduction

HCCI is a Low Temperature Combustion (LTC) mode for internal combustion engines used to reduce NO_X, particulate matter emissions and fuel consumption [1]. HCCI combustion timing control is difficult [1] and several techniques have been developed and implemented for combustion timing control in HCCI engines including, intake air heating [2], variable compression ratio [3], dual fuels [4], water injection [5], Variable Valve Timing (VVT) [6]–[8] and Exhaust Gas Recirculation (EGR) [9]. VVT shows potential among these strategies since it achieves fast cycle-by-cycle control response and reduces residual gas heat loss [6], [10]. VVT changes the effective compression ratio and the amount of trapped residual gas cycle by cycle, both of which have a strong effect on HCCI combustion timing.

HCCI Combustion timing control is important as it affects engine fuel consumption, energy distribution, and emissions [11]. Several control strategies with various levels of complexities have been developed for HCCI load and combustion timing control in the literature. In [4], a Discrete Sliding Mode Controller (DSMC) coupled with a Kalman filter is designed to control combustion timing by varying the auto-ignition properties of the fuel using two Primary Reference Fuels (PRFs) while a feed-forward controller is used for load control [12]. A two-input two-output H_2 controller is developed based on a physics based two-state model for peak cylinder pressure and combustion timing control in [13]. The actuators are IVC and EVC timings and the controller is implemented in a HCCI engine. A three region switching LQR controller is developed and implemented in [14] to track combustion timing using EVC timing as the main actuator. The controller is based on a model developed in [15] and the model is linearized around three different operating points that covers wide HCCI operating range. In [16], LQG, MPC and PID controllers are developed based on identified models and are implemented in a six-cylinder heavy duty engine for cycle by cycle control of combustion timing. Two different actuators are used for combustion timing control including dual fuel and variable valve timing. IVC timing is varied as the valve timing strategy as it changes the effective compression ratio. It is found that variable valve timing has more direct control of combustion timing than the dual-fuel. The MPC shows better performance in load and combustion timing control compared to the PID and LQR. MPC is designed in [6] based on a five-state physical model for output work and combustion timing control with split fuel injection and valve timing as main actuators. The MPC developed in [6] is implemented in a multi-cylinder HCCI engine [17] for load and combustion timing control. An output disturbance estimator is used to compensate the non-modeled cylinder to cylinder cross talk.

In this paper, MPC with Laguerre function [10], [18] is developed for load and combustion timing control of a single cylinder HCCI engine. This approach simplifies the conventional MPC algorithm used in [6], [7], [17] and reduces the computation time which is useful for real-time implementation. The MPC is designed based on a linear model obtained by model order reduction of the DPM [10], [19]. The DPM is based on physics and is a powerful tool for engine modeling when the fuel chemical kinetic mechanism is known. Control design is expedited and insights are gained using the DPM compared to immediate experimental testing. VVT with symmetric NVO strategy is used for cycle-by-cycle combustion timing control and fueling rate is the main actuator for output work control [10], [20]. The controller is implemented in a single cylinder Ricardo Hydra Mark III engine equipped with EVVT system [20] with the specifications listed in Table I. The engine has a port fuel injector that injects n-heptane. The results indicate that MPC with Laguerre function has acceptable combustion timing and load tracking performance considering constraints on the actuators and outputs.

TABLE I

ENGINE SPECIFICATIONS

Parameter	Values
Bore × Stroke [mm]	97 × 88.9
Compression Ratio	13.9
Displacement [L]	0.653
Intake Valve Diameter [mm]	36
Exhaust Valve Diameter [mm]	24
Connecting Rod length [mm]	159

TABLE II

ENGINE OPERATING CONDITIONS

Parameter	Values
Engine Speed [rpm]	725 - 825
T_{Intake} [$^\circ C$]	80
P_{Intake}[kPa]	88 - 90
Injected Fuel Energy [$\frac{\text{kJ}}{\text{Cycle}}$]	0.356 - 0.495
T_{cool} [$^\circ C$]	50
Oil temperature [$^\circ C$]	50
Octane Number (ON) [-]	0
EVC [bTDC]	-350° - -300°
IVO [bTDC]	300° - 350°
EVO [bTDC]	-180°
IVC [bTDC]	180°

II. CONTROL ORIENTED MODEL

A Control Oriented Model (COM) is developed by model order reduction of the DPM [10], [19], [20] to capture the valve timing and fueling rates dynamics since the DPM is too complex for real-time model based control. The steps needed to obtain the COM from the DPM using model order reductions are detailed in [10], [20]. The states, inputs and outputs of the COM are

$$\begin{aligned} x_k &= [T_{IVC} \quad \alpha \quad \phi \quad \theta_{50}]^T \\ u_k &= [m_f \times Q_{LHV} \quad \theta_{EVC}]^T \\ y_k &= [\theta_{50} \quad IMEP]^T \end{aligned} \tag{1}$$

where the definition of each variable is listed in section IX. These states have important effects on HCCI combustion [10], [20]. The nonlinear model is then defined as

$$\begin{aligned} x_{k+1} &= F(x_k, u_k) \\ y_k &= G(x_k) \end{aligned} \tag{2}$$

where F and G are nonlinear functions obtained by modeling the HCCI process as set of distinct events, including compression, combustion and expansion. For COM, fuel equivalence ratio, start of combustion, burn duration and indicated mean effective pressure sub-models in [10] are modified as

$$\phi_k = 7 \times 10^{-3} T_{RES,k-1} m_{fuel,k} Q_{LHV} + 0.19 \tag{3}$$

$$\theta_{soc,k} = -0.0047 T_{IVC,k} - 0.9479 \phi_k + 1.9579 \tag{4}$$

$$\Delta\theta_k = 1.17 \theta_{soc,k} + 0.1602 \tag{5}$$

$$\text{IMEP}_k = 0.046 \times T_{IVC,k} \phi_k - 3.88 \tag{6}$$

The parameters in Eqns. 3 to 6 are obtained using DPM [19]. DPM simulations at over 100 engine operating points, between $0.3 \leq \phi \leq 0.5$ and $10 \leq \theta_{EVC} \leq 50$ at constant speed (n=825 RPM) are used for model parametrization. These parameters are obtained by minimizing the root mean square difference between ϕ, θ_{SOC}, $\Delta\theta$, IMEP values obtained from the DPM and Eqns. 3 to 6 [20]. Then F and G in Eqn. 2 are obtained by rearranging the COM equations as detailed in [10], [20].

TABLE III

OPERATING CONDITION USED TO LINEARIZE NONLINEAR COM

T_{IVC}	385.06 K
α	0.23 [-]
ϕ	0.3 [-]
θ_{50}	-1.019 CAD aTDC
$m_f Q_{HV}$	0.39 kJ
n	817 RPM
θ_{EVC}	20 CAD bTDC

For MPC design, the normalized COM is linearized around the operating point listed in Table III. The operating condition listed in Table III is selected based on the measured experimental data in [20] to ensure that the selected point avoids both engine ringing and misfire. The normalized linearized COM state space model is given by

$$\begin{aligned} x_{k+1} &= Ax_k + Bu_k \\ y_k &= Cx_k + Du_k \end{aligned} \tag{7}$$

where the A, B and C matrices for this operating condition are

$$\begin{aligned} A &= \begin{bmatrix} 0.1129 & -0.0005 & 0.0045 & 0.0000 \\ -1.1953 & 0.0048 & -0.0473 & -0.0004 \\ 0.3424 & -0.0014 & 0.0136 & 0.0001 \\ -7.2144 & 0.0288 & -0.2858 & -0.0021 \end{bmatrix} \\ B &= \begin{bmatrix} 0.0002 & -0.0178 \\ 0 & -2.4634 \\ 0.9741 & 0 \\ -6.9582 & 0.7538 \end{bmatrix} \\ C &= \begin{bmatrix} 0 & 0 & 0 & 1 \\ 7.7047 & 0 & 3.4357 & 0 \end{bmatrix} \end{aligned} \tag{8}$$

and D is a zero matrix. All model states are observable and controllable according to Popov-Belevitch-Hautus (PBH) tests [21].

III. CONTROL ORIENTED MODEL VALIDATION

Measurements from the single cylinder engine [20] are used for steady-state validation of both the COM and DPM. Fig. 1(a) shows that COM and DPM have sufficient accuracy for HCCI combustion analysis as they capture combustion timing with average errors of 1.1 and 1.7 CAD respectively. The DPM estimates higher values for IMEP as higher combustion efficiencies are estimated by the DPM [19] (see Fig. 1(b)). The DPM and COM predict IMEP with average errors of 0.25 and 0.38 bar respectively.

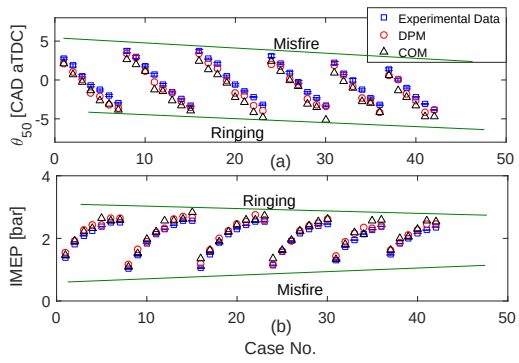

Fig. 1. Steady state model validation of (a) Combustion timing (b) output work [Experiment conditions listed in Table II]

The linearized COM, COM and the DPM [19], [20] are then validated against the experimental data for transient operation as shown in Fig. 2. The computation time of 100 cycles of the DPM on a 3.3 GHz Intel Processor shown in Fig. 2 is approximately 380 sec while the COM only needs 7 msec per 100 engine cycles making the COM suitable for realtime control. The linearized COM shows good accuracy in predicting combustion timing and load with the average errors of 1.7 CAD and 0.38 bar respectively. For real time implementation, MPC with Laguerre function is designed and implemented based on the linearized COM.

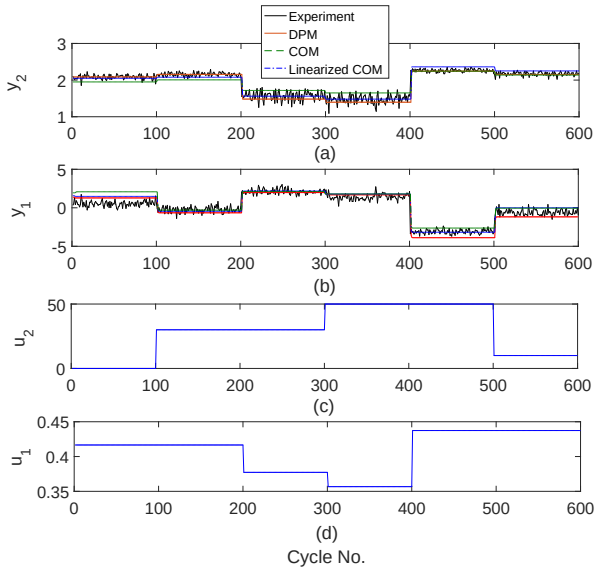

Fig. 2. Transient validation of linearized COM, COM and DPM (a)&(b) outputs $y=[\theta_{50} \quad IMEP]^T$ (c)&(d) inputs $u=[m_f \times Q_{LHV} \quad \theta_{EVC}]^T$ [n=818 RPM, P_{int}=88.9 kPa and T_{int}=86°C]

IV. Controller Design

The controller structure is shown in Fig. 3 and it is based on the algorithm described in [18]. The controller is based on linearized COM and is used to control load and combustion timing. The two main actuators used in this work are valve timing and fueling rate. First, the linearized COM is embedded with two integrators to compensate the model plant mismatch as

$$\begin{aligned} x_{k+1} &= A_e x_k + B_e \Delta u_k \\ y_k &= C_e x_k \end{aligned} \tag{9}$$

where the A_e, B_e and C_e matrices are

$$A_e = \begin{bmatrix} A & 0_4^T \\ CA & I_{2\times 2} \end{bmatrix}$$

$$B_e = \begin{bmatrix} B \\ CB \end{bmatrix} \tag{10}$$

$$C_e = \begin{bmatrix} 0_{2\times 4} & I_{2\times 2} \end{bmatrix}.$$

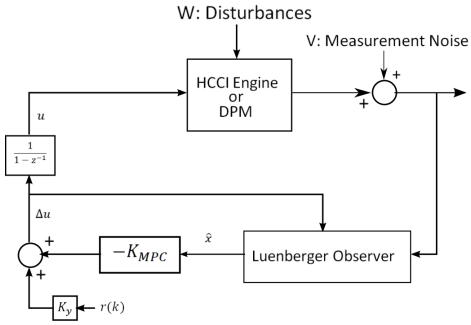

Fig. 3. MPC Structure [18]

Conventional MPC [6], [7], [17] for the case of rapid sampling and complicated process dynamics may require a very large number of parameters, that can lead to poor numerically conditioned solutions and heavy computational load when implemented in realtime [18]. Instead, a Laguerre function approach is used where a set of Laguerre functions are used to capture the control signal dynamic [18] as

$$\Delta u_{k_i+k_f} = L_{k_f}^T \eta \tag{11}$$

where k_i is the initial time, k_f is the future sampling time, L is the Laguerre function and η comprises N Laguerre coefficients. The Laguerre parameters are tuned so that the closed loop eigenvalues of the MPC are identical to the closed loop eigenvalues of the DLQR [18]. The tuned Laguerre parameters are $a_{1,2}$=0.5 and $N_{1,2}$=6 for k_f=10. The prediction horizon of k_f=10 is defined based on transient measurements in [20]. The prediction of the future state at time k_f is defined as

$$x_{k_i+k_f} = A_e^{k_f} x_{k_i} + \phi_{k_f}^T \eta \tag{12}$$

where the parameters η and ϕ_{k_f} are defined [18] as

$$\eta^T = \begin{bmatrix} \eta_1^T & \eta_2^T \end{bmatrix} \tag{13}$$

$$\phi_{k_f}^T = \sum_{j=0}^{k_f-1} A_e^{k_f-j-1} \begin{bmatrix} B_1 L_1(j)^T & B_2 L_2(j)^T \end{bmatrix} \tag{14}$$

for this two-input two-output system. The $\phi_{k_f}^T$ is computed recursively using the convolution sum detailed in [18]. The optimal control cost function is then defined as

$$J = \eta^T \Omega \eta + 2\eta^T \psi x + \sum_{m=1}^{k_f} x^T (A_e^T)^m Q A_e^m x \tag{15}$$

where Ω and ψ are:

$$\Omega = \sum_{m=1}^{k_f} \phi_m Q \phi_m^T + R_L \tag{16}$$

$$\psi = \sum_{m=1}^{k_f} \phi_m Q A_e^m \tag{17}$$

with the weighting matrices R_L and Q. The global optimal solution of the cost function (Eqn. 15) [18] is

$$\eta = -\Omega^{-1} \psi x \tag{18}$$

where the state variables, x, is defined as

$$x = [\Delta x_{k_i+k_f}^T \quad y_{k_i+k_f} - r_{k_i}]^T \tag{19}$$

where r is the reference signal. The closed loop feedback control is then realized as

$$x_{k+1} = (A_e - B_e K_{MPC}) x_k \tag{20}$$

The state feedback control gain, K_{MPC} in Eqn. 20 is then calculated [18] as

$$K_{MPC} = \begin{pmatrix} L_{1,0}^T & 0_2^T \\ 0_1^T & L_{2,0}^T \end{pmatrix} \Omega^{-1} \psi \tag{21}$$

where 0_i^T represents a zero block row vector with identical dimension to $L_{i,0}^T$.

The system constraints defined based on: the absolute limits on the valve events (EVC timing) and fueling rate; the absolute limits on the maximum allowable rate of change of valve events and fueling rate; and the limits on the load and combustion timing to avoid misfire and ringing. The first two constraints are hard constraints and involve the system inputs and are formulated as

$$\Delta u_{min} < \Delta u_k < \Delta u_{max} \tag{22}$$

$$u_{min} < \Delta u_k + u_{k-1} < u_{max} \tag{23}$$

where subscripts *min* and *max* are used to show the minimum and maximum values of the imposed constraints. The last constraint involves the system output and is softened by adding a slack variable, ε to the constraints.

$$y_{min} - \varepsilon < C_e A_e^{k_f} x_k + C_e \phi^T \eta < y_{max} + \varepsilon \tag{24}$$

Hildreth's quadratic programming [18] is then used to minimize the cost function (Eqn. 15) subject to the inequalities in Eqns. 22-24. Table IV lists the minimum and maximum values of the constraints imposed on plant input and output signals.

TABLE IV

MINIMUM AND MAXIMUM VALUES OF THE INPUT AND OUTPUT SIGNALS

	Minimum	Maximum
Injected Fuel Energy [kJ]	0.3	0.5
Injected Fuel Energy Rate [$\frac{\text{kJ}}{\text{Cycle}}$]	-0.1	0.1
θ_{EVC} [CAD bTDC]	0	90
θ_{EVC} Rate [$\frac{\text{CAD}}{\text{Cycle}}$]	-20	20
IMEP [bar]	0.68	2.5
θ_{50} [CAD aTDC]	-1	8

V. LUENBERGER OBSERVER

The linearized COM states of $x_1 = T_{IVC}$ and $x_2 = \alpha$ cannot be measured easily on real engine, so a full state Luenberger observer [21] is designed. The observed state vector $\hat{x}$ is,

$$\hat{x}_{k+1} = A_e \hat{x}_k + K_{ob} [y_k - \hat{y}_k] + B_e \Delta u_k \tag{25}$$

where $\hat{y}$ is the estimated value of the model output and K_{ob} is the Luenberger observer gain. In the experiment, the observer gain is tuned by pole placement to attenuate measurement noise while keeping the transient dynamic fast [21]. The observer accuracy is compared to the experiment for a valve timing step as shown in Fig. 4 where only combustion timing and fuel equivalence ratio are compared as the other two states are not measured. These results indicate that the designed observer estimates the model states with acceptable accuracy.

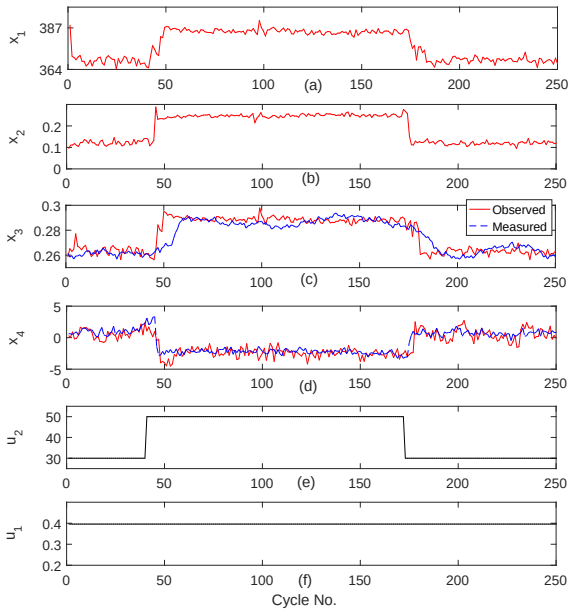

Fig. 4. Comparison of the observer performance in simulation with the measurements, (a)-(d): states $x = [T_{IVC} \quad \alpha \quad \phi \quad \theta_{50}]^T$, (e)-(f): inputs $u = [m_f \times Q_{LHV} \quad \theta_{EVC}]^T$ [n=820 RPM, P_{int}=89.0 kPa and T_{int}=81°C]

VI. MPC PERFORMANCE IN SIMULATION

The controller is verified in simulation using the DPM [20] as a virtual engine. Controller performance without considering constraints on inputs and outputs are shown in Fig. 5 and

MPC with Laguerre function is compared to the conventional MPC [6]. The control horizon and prediction horizon for the conventional MPC are set to 3 and 10 respectively [6], [20]. The average computation time, measured in processor clock cycles, is 1.15 times higher for conventional MPC compared to the MPC with Laguerre function. Both controllers are able to track combustion timing and load setpoint values closely.

MPC with Laguerre function performance considering input and output constraints are shown in Fig. 6. The controller can not track the desired combustion timing before cycle 200 as the EVC timing reaches its maximum constraint. The desired combustion timing and load are changed to 2 CAD bTDC and 2.5 bar respectively after cycle 200. The controller increases the fueling rate to track the desired load, however, it does not track the desired combustion timing since the combustion timing lower limit is set to 1 CAD bTDC. At cycle 300, the desired combustion timing is retarded to 3 CAD aTDC and the desired load is increased to 3 bar. The controller tracks the desired combustion timing by retarding the EVC timing to TDC, however, it does not track the desired load trajectory due to the constraint and maintains the load at the maximum limit of 2.5 bar. The controller has acceptable disturbance rejection properties as detailed in [10], [20] and performs well despite the measurement noise in the feedback signal as discussed in [10], [20].

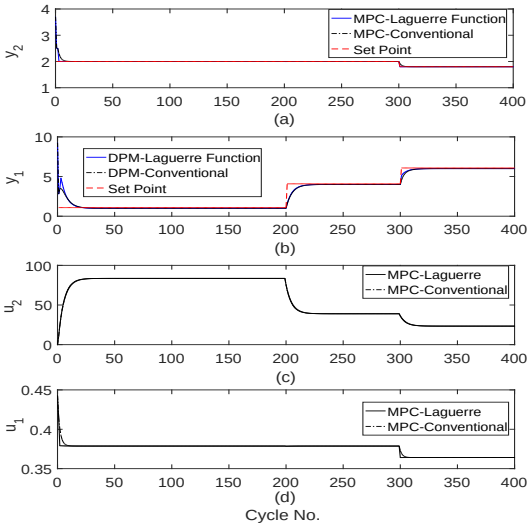

Fig. 5. MPC - Controller performance without constraints simulation: (a) & (b) system outputs $y = [\theta_{50} \quad IMEP]^T$ (c) & (d) controller outputs $u = [m_f \times Q_{LHV} \quad \theta_{EVC}]^T$ [n=825 RPM, P_{int}=95 kPa and T_{int}=80^{o}C]

VII. MPC Implementation on Single Cylinder Research Engine

The controller is implemented in real-time on a single cylinder research engine [20]. The measured cylinder pressure is used to calculate combustion timing that is required as feedback to the controller. MPC with Laguerre function is implemented on the engine through dSPACE ControlDesk and Matlab real-time workshop. The engine is controlled

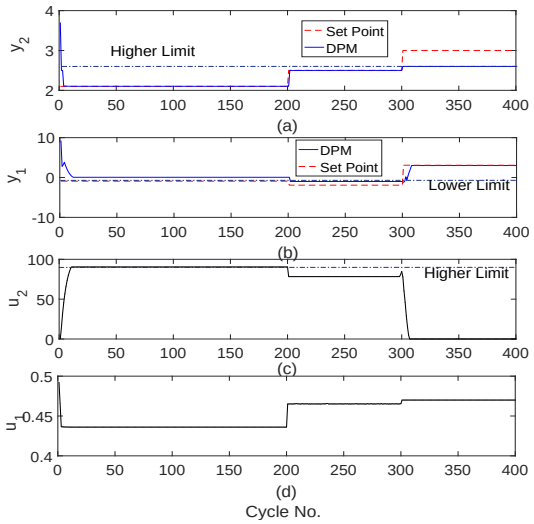

Fig. 6. MPC - Controller performance with constraints simulation: (a) & (b) system outputs $y = [\theta_{50} \quad IMEP]^T$ (c) & (d) controller outputs $u = [m_f \times Q_{LHV} \quad \theta_{EVC}]^T$ [n=825 RPM, P_{int}=95 kPa and T_{int}=80^{o}C]

mainly at low loads and desired combustion timing is determined based on measurements in [20] to keep both thermal and combustion efficiencies high ($\eta_{th} \simeq 33\%$, $\eta_{comb} \simeq 90\%$). It is important to note that even if the output power is low, efficient engine control strategy still required to save fuel [22].

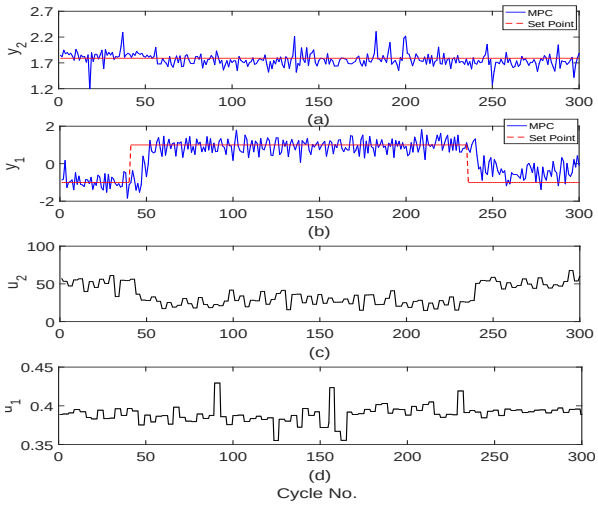

Fig. 7. Experiment - MPC implementation, (a) & (b): System outputs $y = [\theta_{50} \quad IMEP]^T$, (c) & (d): Controller Outputs $u = [m_f \times Q_{LHV} \quad \theta_{EVC}]^T$ [n= 788 RPM, P_{int}=89.0 kPa and T_{int}=82^{o}C]

Fig. 7 shows the MPC controller performance for combustion timing tracking at constant load. The desired combustion timing is retarded by 2 degrees at cycle 40 and then it returned back to its original value at cycle 236. MPC shows good performance in combustion timing tracking by adjusting EVC timing. Actuator fluctuations are attributed to the fast model transient dynamics and the integral action. The MPC is tested to track load at constant combustion timing in

Fig. 8. The MPC can track load fairly accurately considering constraints on the fueling rate and valve timing (the dash-dot lines in Fig. 8 (c) and (d) show the actuators' limits). As shown in Fig. 8 (d), the fueling rate reaches the lower limit at cycles 49 and 99 and the controller can keep the fueling rate within the actuators' limits. The desired IMEP is reduced from 2 bar to 1.4 bar at cycle 44 and the controller is able to track this by reducing the fueling rate. The controller modulates the EVC timing to trap more residual gas and keep the combustion timing at 1 CAD aTDC. The desired IMEP is returned back to 2 bar, its original value at cycle 150. The controller increases the fueling rate to meet the desired load and EVC timing is retarded to TDC to trap less residual gas and keep the combustion timing constant.

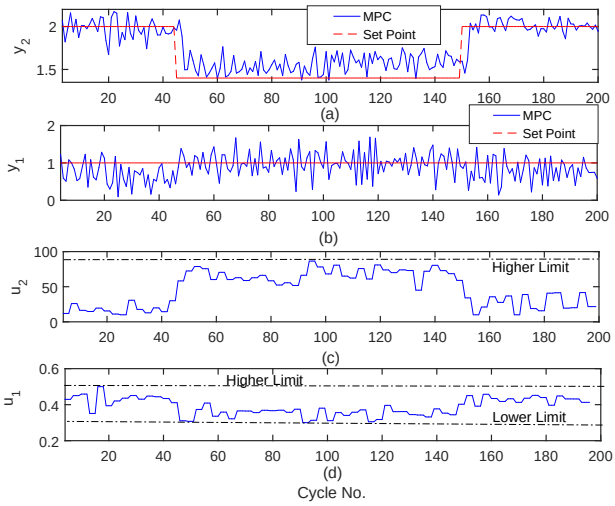

Fig. 8. Experiment - MPC implementation, (a) & (b): System outputs $y = [\theta_{50} \quad IMEP]^T$, (c) & (d): Controller Outputs $u = [\, m_f \times Q_{LHV} \quad \theta_{EVC}]^T$ [n= 758 RPM, P_{int}=90.7 kPa and T_{int}=85°C]

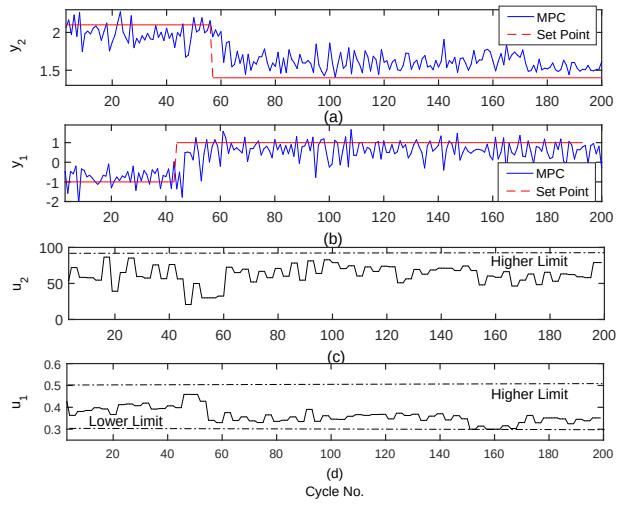

Fig. 9. Experiment - MPC implementation, (a) & (b): System outputs $y = [\theta_{50} \quad IMEP]^T$, (c) & (d): Controller Outputs $u = [\, m_f \times Q_{LHV} \quad \theta_{EVC}]^T$ [n= 765 RPM, P_{int}=89.5 kPa and T_{int}=83°C]

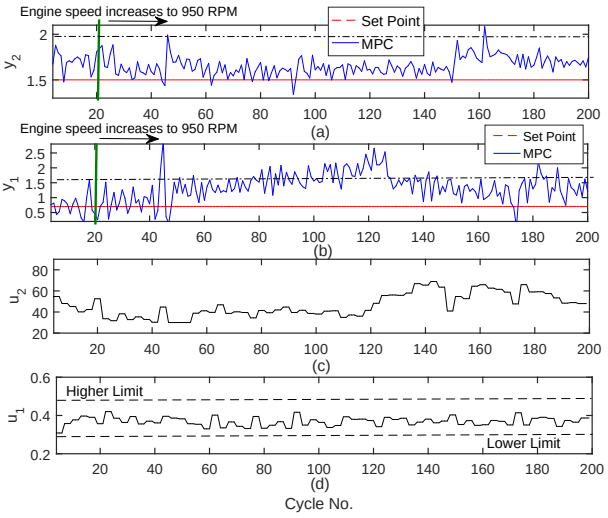

Fig. 10. Experiment - MPC implementation: (a) & (b): System outputs $y = [\theta_{50} \quad IMEP]^T$, (c) & (d): Controller Outputs $u = [\, m_f \times Q_{LHV} \quad \theta_{EVC}]^T$ [P_{int}=89 kPa and T_{int}=81°C]

Fig. 9 shows the controller performance in tracking load and combustion timing when both reference values are changed. First, desired combustion timing is retarded to 1 CAD aTDC at cycle 44. The controller retards the EVC timing to TDC to trap less residual gas and retards the combustion timing. Then, the desired IMEP is reduced at cycle 56 to 1.4 bar. Fueling rate is reduced by the controller to track the desired load. The combustion timing tends to be retarded at lower fueling rates, hence, the controller modulates the trapped residual gas by advanced EVC timing and keep combustion timing constant at 1 CAD aTDC. At cycles 151, 157 and 166, the fueling rate reaches the lower actuator limit as shown in Fig. 9 and the controller shows good performance in keeping the fueling rate within the defined constraints in Table IV. Fig. 10 shows engine speed disturbance rejection properties of MPC by examining the output constraints. Engine speed is increased at cycle 22 from 725 to 950 RPM and the combustion timing retards with increasing engine speed. The constraints are imposed on both combustion timing and load. Fig. 10 (a) and (b) shows the load and combustion timing higher limits as dash-dot lines. The combustion timing reaches the higher limit at cycle 78 and then cross the limit (see Fig. 10 (b)). The output constraints are activated at cycle 117 and the controller increases NVO duration to return the combustion timing back to its initial value with trapping more residual gas (see Fig. 10 (c)). The controller does not change the fueling rate as the IMEP is almost constant with an increase in engine speed. The constraint violation between cycles 78 and 117 is due to the slack variable in optimization algorithm. Fig. 10 shows the controller is able to regulate the combustion timing to the reference value and keep the combustion timing within the limits defined by the constraints.

VIII. Conclusions

A nonlinear control oriented model is developed and validated for cycle by cycle load and combustion timing control in HCCI engine. The model shows acceptable accuracy in predicting HCCI output work and combustion timing. The model is then linearized around one operating point and the linearized model is used to design MPC with Laguerre functions. MPC with Laguerre functions is demonstrated in real-time and shows a modest improvement in computational load over standard MPC. The developed controller shows acceptable performance for cycle by cycle control of combustion timing and load in simulation considering constraints on inputs and outputs. Luenberger observer is used to implement the controller and the model is augmented with two integrators to compensate model/plant mismatch. The implemented MPC shows acceptable performance in tracking step changes in load and combustion timing while considering constraints on the inputs and outputs. Both the nonlinear control oriented model and the controller have a simple structure and can be easily reformulated for other fuels including bio-fuels.

IX. Definitions/Abbreviations

α	Residual Gas Fraction at IVC [-]
$\Delta\theta$	Burn Duration [rad]
ϕ	Fuel Equivalence Ratio [-]
θ_{50}	Crank Angle of Fifty Percent Mass Fraction Burned [CAD aTDC]
θ_{SOC}	Start of Combustion Timing [rad aTDC]
θ_{EVC}	Crank Angle of EVC [CAD bTDC]
aTDC	after Top Dead Center
bTDC	before Top Dead Center
CAD	Crank Angle Degree
EVO	Exhaust Valve Opening
EVVT	Electromagnetic Variable Valve Timing
HCCI	Homogeneous Charge Compression Ignition
IMEP	Indicated Mean Effective Pressure [bar]
IVC	Intake Valve Closing
IVO	Intake Valve Opening
LQG	Linear Quadratic Gaussian
LQR	Linear Quadratic Regulator
m_f	Mass of Fuel Injected Per Cycle [kg]
MPC	Model Predictive Control
NVO	Negative Valve Overlap
Q_{LHV}	Fuel Lower Heating Value [$\frac{\text{kJ}}{\text{kg}}$]
SOC	Start of Combustion
T_{IVC}	Temperature at Intake Valve Closing [k]
T_{RES}	Residual Gas Temperature
TDC	Top Dead Center
u	Model Inputs
x	Model States
y	Model Outputs

References

[1] H. Zhao, *HCCI and CAI engines for the automotive industry*. CRC Press, 2006.

[2] P. M. Najt and D. E. Foster, "Compression-ignited homogeneous charge combustion," *SAE Int. J. Engines*, SAE Technical Paper 830264, 1983. doi:10.4271/830264.

[3] G. Haraldsson, P. T. l, B. Johansson, and J. Hyvönen, "HCCI Combustion Phasing with Closed-Loop Combustion Control Using Variable Compression Ratio in a Multi Cylinder Engine," SAE Technical Paper 2003-01-1830, 2003, 05 2003. doi: 10.4271/2003-01-1830.

[4] M. Bidarvatan, M. Shahbakhti, S. Jazayeri, and C. Koch, "Cycle-to-cycle modeling and sliding mode control of blended-fuel HCCI engine," *Control Engineering Practice*, vol. 24, no. 0, pp. 79 – 91, 2014. doi: 10.1016/j.conengprac.2013.11.008.

[5] Y. Iwashiro, T. Tsurushima, Y. Nishijima, Y. Asaumi, and Y. Aoyagi, "Fuel Consumption Improvement and Operation Range Expansion in HCCI by Direct Water Injection ," SAE Technical paper 2002-01-0105, 2002.

[6] N. Ravi, H.-H. Liao, A. F. Jungkunz, A. Widd, and J. C. Gerdes, "Model predictive control of HCCI using variable valve actuation and fuel injection," *Control Engineering Practice*, vol. 20, no. 4, pp. 421 – 430, 2012. Special Section: IFAC Symposium on Advanced Control of Chemical Processes - ADCHEM 2009, doi: 10.1016/j.conengprac.2011.12.002.

[7] J. Bengtsson, P. Strandh, R. Johansson, P. Tunestål, and B. Johansson, "Model predictive control of Homogeneous Charge Compression Ignition (HCCI) engine dynamics," in *Computer Aided Control System Design, 2006 IEEE International Conference on Control Applications, 2006 IEEE International Symposium on Intelligent Control, 2006 IEEE*, pp. 1675–1680, Oct 2006. doi: 10.1109/CACSD-CCA-ISIC.2006.4776893.

[8] G. Shaver, M. Roelle, and J. Gerdes, "Decoupled control of combustion timing and work output in residual-affected HCCI engines," in *Proceedings of the 2005 American Control Conference*, pp. 3871–3876 vol. 6, June 2005. doi: 10.1109/ACC.2005.1470578.

[9] J. M. Kang and M. Druzhinina, "HCCI engine control strategy with external EGR," in *Proceedings of the 2010 American Control Conference*, pp. 3783–3790, June 2010. doi: 10.1109/ACC.2010.5531558.

[10] K. Ebrahimi and C. Koch, "Model Predictive Control for Combustion Timing and Load Control in HCCI Engines," SAE International, SAE 2015-01-0822, 2015.

[11] K. Ebrahimi and C. Koch, "Symmetric Negative Valve Overlap Effects on Energy Distribution of a Single Cylinder HCCI Engine," in *WCX: SAE World Congress Experience,SAE 2018-01-1250*, SAE International, Apr 2018.

[12] M. Bidarvatan and M. Shahbakhti, "Two-Input Two-Output Control of Blended Fuel HCCI Engines," in *SAE Technical Paper*, SAE Technical Paper, 2013-01-1663, 2013, doi: 10.4271/2013-01-1663.

[13] G. Shaver, M. Roelle, and J. Gerdes, "A two-input two-output control model of HCCI engines," in *Proceedings of the 2006 American Control Conference*, June 2006. doi: 10.1109/ACC.2006.1655401.

[14] H.-H. Liao, A. Widd, N. Ravi, A. F. Jungkunz, J.-M. Kang, and J. C. Gerdes, "Control of recompression HCCI with a three region switching controller," *Control Engineering Practice*, vol. 21, no. 2, pp. 135 – 145, 2013.

[15] N. Ravi, M. Roelle, H. H. Liao, A. Jungkunz, C. F. Chang, S. Park, and J. Gerdes, "Model-Based Control of HCCI Engines Using Exhaust Recompression," *IEEE Transactions on Control Systems Technology*, vol. 18, pp. 1289–1302, Nov 2010.

[16] J. Bengtsson, P. Strandh, R. Johansson, P. Tunestl, and B. Johansson, "Hybrid control of homogeneous charge compression ignition (HCCI) engine dynamics," *International Journal of Control*, vol. 79, no. 5, pp. 422–448, 2006.

[17] S. M. Erlien, A. F. Jungkunz, and J. C. Gerdes, "Multi-Cylinder HCCI Control With Cam Phaser Variable Valve Actuation Using Model Predictive Control.," in *Proceedings of the 2012 ASME Dynamic Systems and Control Conference*, vol. 2, pp. 823 – 832, 2013. doi:10.1115/DSCC2012-MOVIC2012-8585.

[18] L. Wang, *Model predictive control system design and implementation using MATLAB*. Advances in industrial control, London : Springer, c2009., 2009.

[19] K. Ebrahimi, A. Schramm, and C. R. Koch, "A Control Oriented Model with Variable Valve Timing for HCCI Combustion Timing Control," in *SAE Paper 2013-01-0588*, p. 12, 2013. doi: 10.4271/2013-01-0588.

[20] K. Ebrahimi, *Model Based Control of Combustion Timing and Load in HCCI Engines*. PhD thesis, University of Alberta, 2016.

[21] C.-T. Chen, *Linear system theory and design*. New York: Oxford University Press, 1999.

[22] I. Ekoto, B. Wolk, and W. Northrop, "Energy analysis of low-load low-temperature gasoline combustion with auxiliary-fueled negative valve overlap," *SAE Int. J. Engines*, vol. 10, 2017.